

21cm Radio-Astrophysics: Rotation Curves & Dark Matter

Francisca Vasconcelos*
MIT Department of Physics
(Dated: December 4, 2019)

In this work, the MIT JLAB Small Radio Telescope (SRT) is used to measure 1420.4MHz radio-wave emissions of neutral hydrogen clouds in the Milky Way Galaxy. Several galactic coordinates are measured and analysis is performed to determine the corresponding red-shift at that distance from the galactic center. This is used to estimate the rotational velocity of matter for varying rotational curves. The resulting observations deviate from the Keplerian model of the galaxy, instead providing evidence for the proposed dark matter model.

I. INTRODUCTION

As early as 1884, Lord Kelvin estimated that the mass of the galaxy was greater than the mass of visible stars [1]. Since then, several independent scientists have postulated and gathered experimental evidence for the existence of “dark matter.” This form of matter is believed not to interact with electromagnetic waves and is thus undetectable by currently existing astronomical instruments. Furthermore, dark matter is estimated to comprise 85% of matter in the universe. This experiment aims to measure the velocity of matter for different rotation curves throughout the Milky Way galaxy. These measurements are compared to the expected Keplerian velocity curve and used as observational evidence to support the dark matter model.

II. THEORY

II.1. Hydrogen Spin-Flips

Neutral hydrogen plays a central role in Big Bang cosmology because of its prevalence throughout the universe. In fact, it is assumed to be scattered uniformly throughout our galaxy, populating the spiral arms of the Milky Way. From quantum mechanics, it is known that the proton and electron spins of neutral hydrogen can have two different configurations: symmetric and anti-symmetric. Due to the nature of the electron and proton wavefunctions, the anti-symmetric configuration has a slightly lower energy than the symmetric configuration. Thus, neutral hydrogen will occasionally transition from the symmetric configuration to the more energetically favorable anti-symmetric configuration. This transition is known as a “spin-flip” and emits electromagnetic radiation at 1420.4MHz (21cm wavelength).

These emissions are used in radio-astronomy to observe large neutral hydrogen clouds in otherwise “invisible” portions of the galaxy. However, given that these hydrogen clouds are dynamic, an individual hydrogen particle can move with a different velocity from the ensemble,

causing Doppler shifts in the observed frequency and a broadened spectra of frequency measurements. This feature, known as *thermal broadening*, is characterized as a source of uncertainty and used to distinguish noise from actual spectral peaks.

II.2. Structure of the Milky Way Galaxy

The Milky Way Galaxy is a large spiral galaxy consisting of six main components: the nucleus, central bulge, disk, spiral arms, spherical component, and massive halo [2]. For the purposes of this experiment, we are primarily concerned with the spiral arms. Despite the logarithmic form of these arms, a simplified model of the galaxy is used, in which matter rotates in concentric rings surrounding the galactic center, as illustrated in Fig 1. Our solar system lies in a spiral arm, $R_{\odot} = 8.7 \pm 0.5\text{kpc}$ from the galactic center, rotating at a velocity of $V_{\odot} = 220 \pm 20\text{km/sec}$ [3].

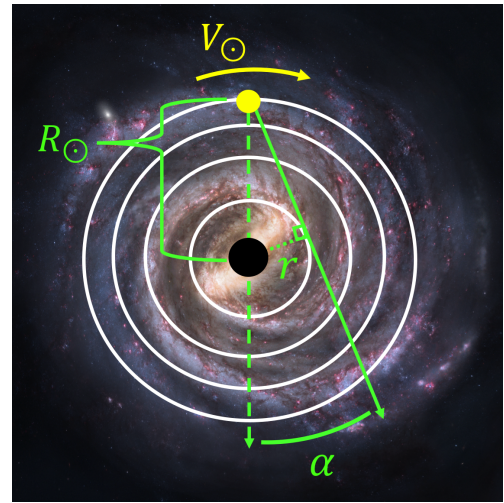


FIG. 1. The spiral arms of the Milky Way Galaxy can be approximated as series of concentric rings. For a galactic coordinate (α), given the distance between the solar system and galactic center (R_{\odot}), we can calculate the radius (r) of the tangential ring. Utilizing the rotation velocity of the solar system (V_{\odot}) and measures of the Doppler shifted 21cm line, the maximum velocity at radius r can be predicted.

* francisc@mit.edu

II.2.1. Keplerian & Dark Matter Models

The Keplerian model uses Newtonian mechanics to predict the velocity of mass distributed throughout the spiral arms. For distances less than $\sim 5\text{kpc}$, the velocity is $\propto r$. This regime is hard to model since the mass distribution is not uniform. However, we are not too interested in this regime, because previous experiments have demonstrated that observational data follows existing Keplerian models fairly well [4].

On the other hand, for distances greater than $\sim 5\text{kpc}$, the Keplerian model predicts,

$$v = \sqrt{\frac{GM_{\odot}}{r}}, \quad (1)$$

where $G \approx 6.67408 \times 10^{-20}\text{m}^3/\text{kg sec}$ is the gravitational constant and $M_{\odot} = \frac{R_{\odot}V_{\odot}^2}{G} \approx 1.81766 \times 10^{41}\text{kg}$ is the mass distributed in the spiral arms. However, the Dark Matter model postulates the existence of non-luminous matter in the outskirts of the galaxy. This causes the rotational velocity to flatline for increasing r , deviating from the Keplerian model.

II.3. Galactic Rotation Curves

The velocity of galactic matter for a given r can be calculated by looking for the max red-shift at the galactic coordinate, α , tangential to the rotation curve with radius r . The relationship between galactic coordinate and radius is

$$r = R_{\odot} \sin\left(\frac{\alpha\pi}{180^\circ}\right), \quad (2)$$

with corresponding velocity

$$V(r) = V_{max} + V_{\odot} \sin\left(\frac{\alpha\pi}{180^\circ}\right). \quad (3)$$

V_{max} is the maximum radial velocity along our line of sight, calculated using the Doppler shift equation,

$$V_{max} = \frac{f_0 - f_{red}}{f_0} c - V_{lsr}, \quad (4)$$

where $f_0 = 1420.4\text{MHz}$, f_{red} is the maximally red-shifted frequency of the 1420.4 line, c is the speed of light, and V_{lsr} is the velocity with respect to the local standard of rest (accounts for movement of Earth around the sun).

III. EXPERIMENTAL SETUP

III.1. Measurement Chain

The MIT JLAB Small Radio Telescope (SRT) has a parabolic 1.14m dish and a beam width of 7° . The

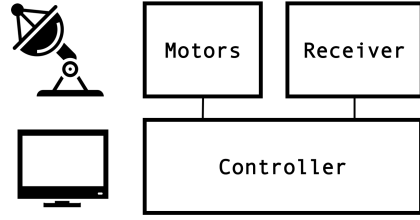


FIG. 2. Although the MIT SRT has a fairly complicated measurement chain, at a high level we can use a computer to control the orientation of the antenna, which receives and filters radiowaves in the frequency band surrounding 1420.4MHz.

motors of the antenna can be controlled from a Java GUI/scripting applet, that allows the user to specify galactic coordinates or azimuth/elevation. Radio frequencies received in the dish are reflected into a feed horn and passed through a low noise amplifier (24 dB gain) followed by a 40MHz band-pass filter. The signal is reported back to the computer controller as an antenna temperature, which is proportional to the power of the signal. A high-level diagram of the measurement chain is depicted in Fig 2. For more detailed information refer to the JLAB and SRT Manuals [5].

III.2. Measurement Procedure

In order to determine rotational velocities at several distances from the galactic center, multiple (≥ 10) measurements of 10min were made at each of the galactic coordinates $\alpha \in \{0^\circ, 5^\circ, 10^\circ, \dots, 80^\circ, 85^\circ, 90^\circ\}$. In this portion of the galaxy, the spiral arms rotate *away* from the antenna, which is why we look for the *red-shift*.

In order to measure the *thermal broadening*, ten 10min measurements were performed for $\alpha = 180^\circ$, in which the antenna was pointed directly opposite from the galactic center. At this galactic coordinate, any observed hydrogen clouds rotate perpendicular to the line of sight and no Doppler shift should be attributed to rotational velocity, but instead to fluctuating velocities of hydrogen particles in the cloud.

IV. DATA ANALYSIS

IV.1. Background Subtraction

Usually, background noise can be determined by pointing the antenna perpendicular to the plane of the galaxy (into empty space). However, in our measurements, the calibration curves had larger signal amplitude than those measured within the galactic plane, meaning there was probably a noise source in the “empty” area of the sky. So, we instead modeled the background noise as linear. After averaging all the measurements for a given galactic coordinate (and propagating the Poissonian measurement uncertainties), a linear fit of the data was per-

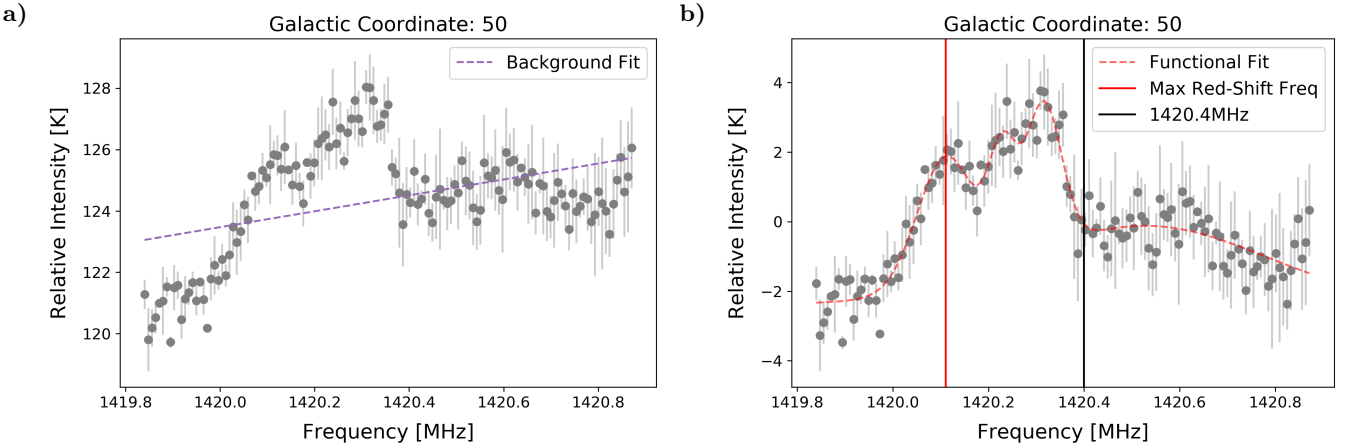


FIG. 3. (a) After averaging the frequency measurements for galactic coordinate $\alpha = 50^\circ$, a linear fit is performed to model the background noise. (b) The noise model is subtracted from the data. Four Gaussians and a linear offset are fit to the data to determine the peak corresponding to maximal red-shift of the 1420.4MHz spectral emission of hydrogen.

formed, as shown in Fig 3, and subtracted from the signal. The fit parameters for each galactic coordinate are reported in Appendix A.

IV.2. Thermal Broadening Spread

As discussed in the *Theory* section, thermal broadening is important for characterizing the expected spread of all observed spectral emission lines and distinguishing these peaks from noise in the signal. After averaging, error propagating, and subtracting background from our $\alpha = 180^\circ$ measurements, the spread induced by thermal broadening was estimated by performing a Gaussian curve-fit. In order to improve the quality of this fit, a linear offset component was added, making the fit equation,

$$f(x) = \frac{A}{\sigma\sqrt{2\pi}} e^{-\frac{(x-\mu)^2}{2\sigma^2}} + B, \quad (5)$$

with the four free parameters: A , B , μ , and σ . This fit, as shown in Fig 4, had $\chi^2 = 200.859$, $df = 132$, and a $\chi_r^2 = 1.522$. The predicted mean of this distribution was fairly close to the expected 1420.4MHz, with $\mu = 1420.378 \pm 0.004$ MHz. Finally, the main value of interest was the spread, $\sigma = 0.070 \pm 0.004$ MHz.

IV.3. Determining Max Red-Shift

In order to determine the maximum frequency redshift, we performed a fit of four Gaussians and a linear offset for each of the galactic coordinate frequency measurements (0° to 90°). This is similar to the thermal broadening fit described by Eqn 5, but with three additional Gaussian terms, meaning 13 total free parameters. Some manual testing was performed for the initialization, to ensure a good fit for each galactic coordinate curve.

In order to determine the maximally red shifted frequency, the output Gaussian fit parameters were assessed. Initially the Gaussian with the smallest value of

μ (the lowest frequency peak) was considered the peak of interest. However, it was discovered that, for several fits, some Gaussians would be far more narrow or broad than a spectral peak, due to over-fitting. Given the expected peak width due to thermal broadening (as discussed in the previous section), these over-fitted peaks were filtered out by imposing a threshold on the σ value of the minimum peak. An example of the fit and predicted minimum frequency for $\alpha = 50^\circ$ is plotted in Fig 3. For similar plots of the other galactic coordinates as well a table of the fit parameters, refer to *Appendix A*.

IV.4. Fitting Models

Using Eqn 3 and Eqn 4, these predicted red-shifted frequencies are converted into rotational velocities. Using Eqn 2, the radial distance of this rotating matter from the galactic center is calculated. By repeating this process

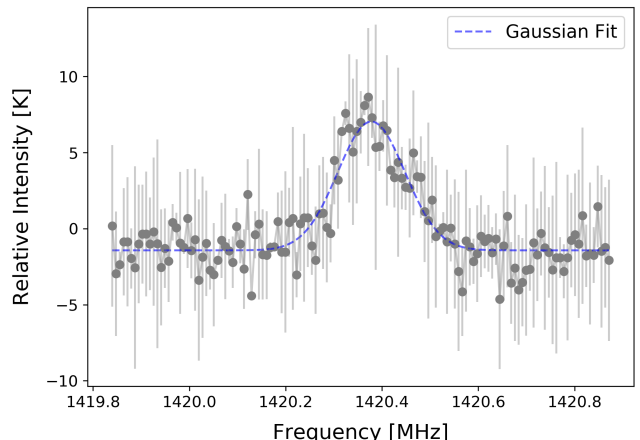


FIG. 4. Averaged frequency data collected at galactic coordinate $\alpha = 180^\circ$. A Gaussian with a linear offset was fit to the curve to determine the spread induced by thermal broadening.

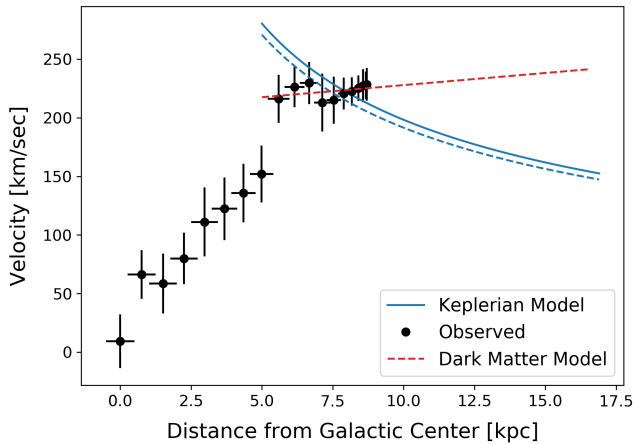


FIG. 5. Velocities calculated from observations using the MIT JLAB SRT are plotted in black. For $r \geq 5\text{kpc}$, this data was fit to both the Keplerian and dark matter models (dashed lines). The theoretically predicted Keplerian curve is also plotted (solid line).

for all the measured galactic coordinates, we create the plot shown in Fig 5. Uncertainty along the radial axis for each point results primarily from error propagation of the uncertainty in R_\odot . Uncertainty along the velocity axis results primarily from error propagation in V_\odot . As described earlier, the mean frequency observed in the thermal broadening measurement was extremely close to the anticipated 1420.4MHz value, so the systematic uncertainty due to miscalibration was deemed negligible.

IV.5. Dark Matter Model

As discussed in the *Theory* section, the dark matter model predicts a linear velocity trend for rotation curves of radius greater than $\sim 5\text{kpc}$. Thus, a linear fit on all of measured data points with $r \geq 5\text{kpc}$ returned a slope of $2.069 \pm 1.688 \frac{\text{km}}{\text{sec kpc}}$ with offset $207.178 \pm 12.924 \frac{\text{km}}{\text{sec}}$. This is depicted with a red dashed line in Fig 5 and the goodness of fit metrics are reported in Table I.

IV.6. Keplerian Model

As discussed in the *Theory* section, there is a well described model for the Keplerian view of the galaxy. We plotted, in solid blue in Fig 5, the curve described by Eqn 1 using our calculated value of M . Although the

data does not appear to fit this model particularly well, we wanted to compare the fit to that of the dark matter model. Thus, we performed a fit of data points with $r \geq 5\text{kpc}$ to the curve the Keplerian curve, multiplied by \sqrt{A} , where A is a free re-scaling parameter. The outcome of this fit is plotted in the dashed blue line, with $A = 0.933 \pm 0.051$. The goodness of fit metrics are reported in Table I.

TABLE I. Fit characteristics for the dark matter and Keplerian models for observed data points with $r \geq 5\text{kpc}$.

Model	χ^2	df	χ_r^2	$Pr(\chi^2)$
Dark Matter	0.857	10	0.086	.9999
Keplerian	16.755	10	1.676	.0800

V. RESULTS & CONCLUSIONS

The theoretical Keplerian curve did not appear to fit the observed data well. By performing a fit with a re-scaling factor (to account for potential false assumptions in calculating M) we could compare this model quantitatively to the dark matter model. The goodness of fit results presented in Table I, especially the high $Pr(\chi^2)$ of the linear dark matter model relative to the Keplerian model, gives strong reason to believe that after 5kpc rotational velocity is constant and not $\propto \frac{1}{\sqrt{r}}$.

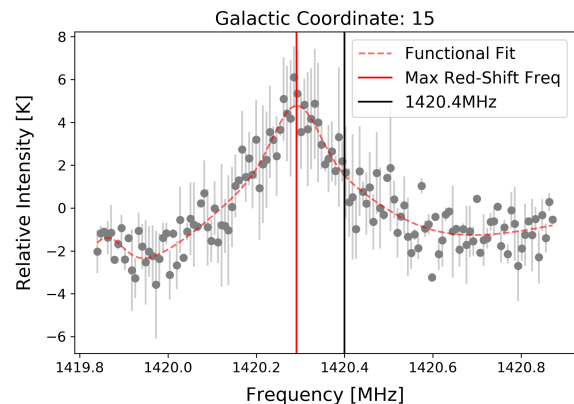
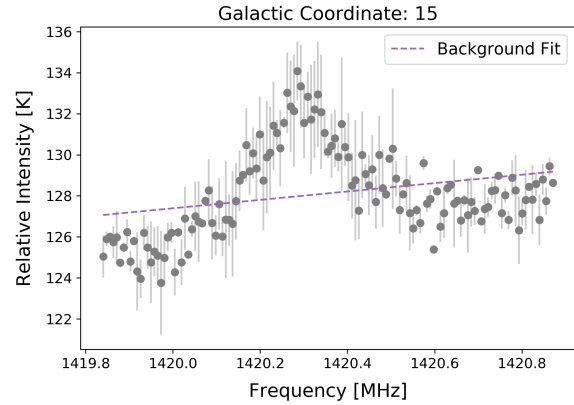
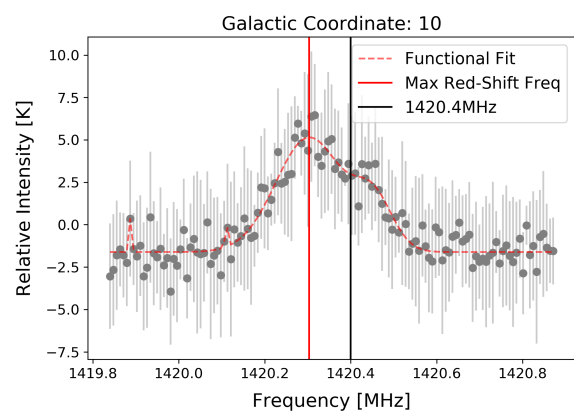
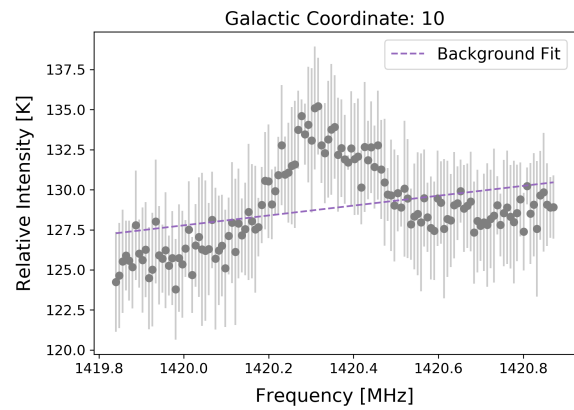
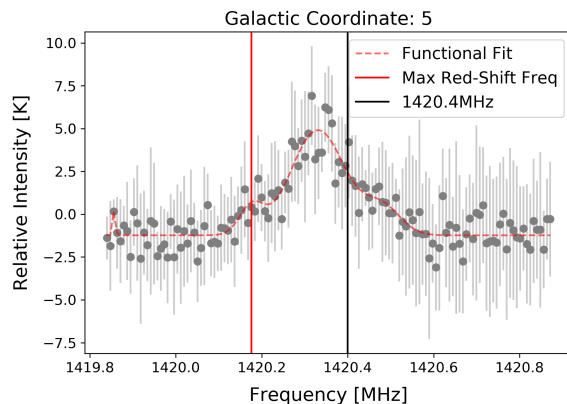
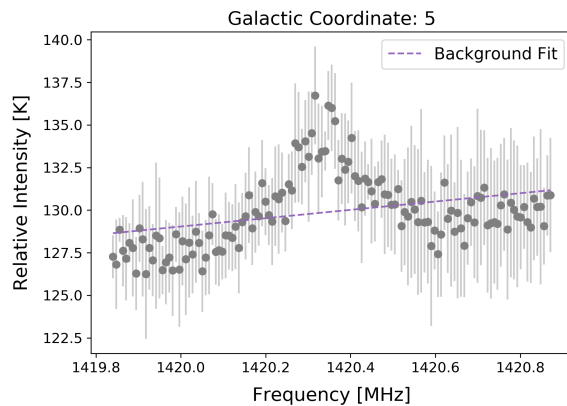
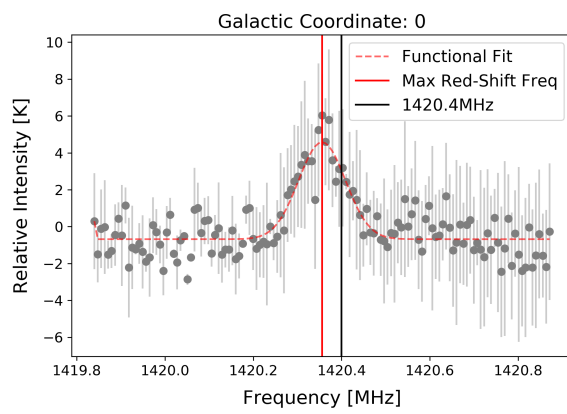
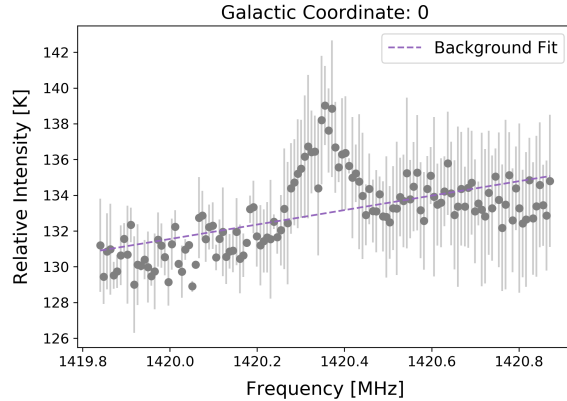
In conclusion, by using the MIT JLAB SRT to measure the 1420.4MHz frequency band, we were able to observe the maximum red-shift of neutral hydrogen cloud emissions. This enabled calculation of the expected rotational velocity of matter at several distances from the galactic center, in our concentric rings model of the Milky Way galaxy. By comparing data points with $r \geq 5\text{kpc}$ to existing Keplerian and dark matter models of the galaxy, we found our data to be strong evidence in favor of the dark matter model. Whether there truly is non-luminous matter prominent in the outskirts of the Milky Way spiral arms, or if there is some other unknown physical reason for our observations, remains an open question.

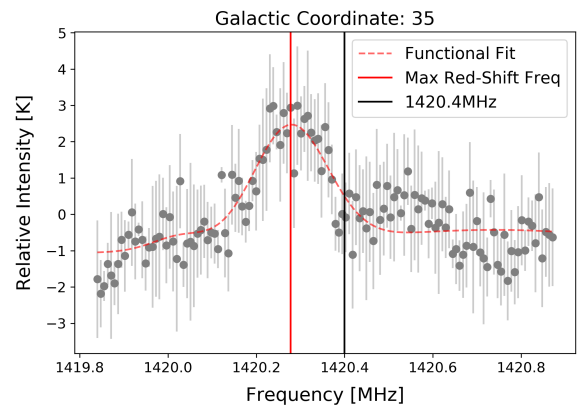
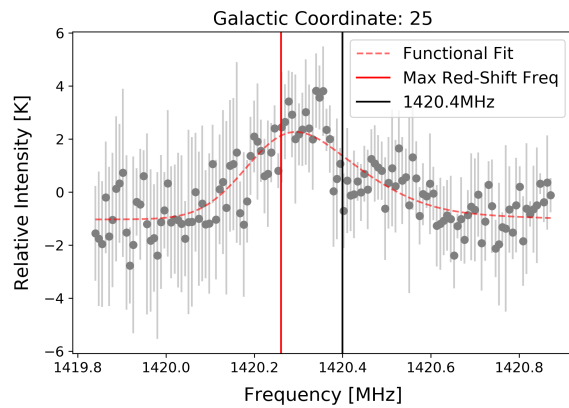
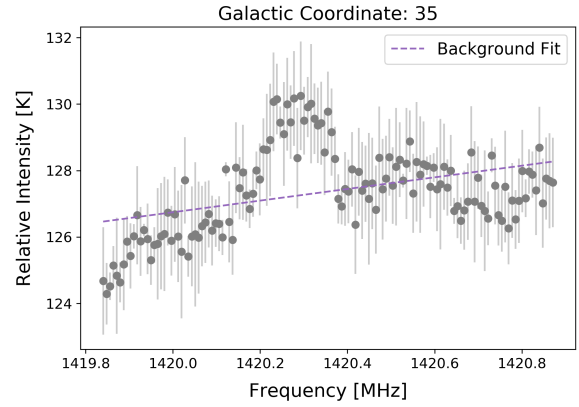
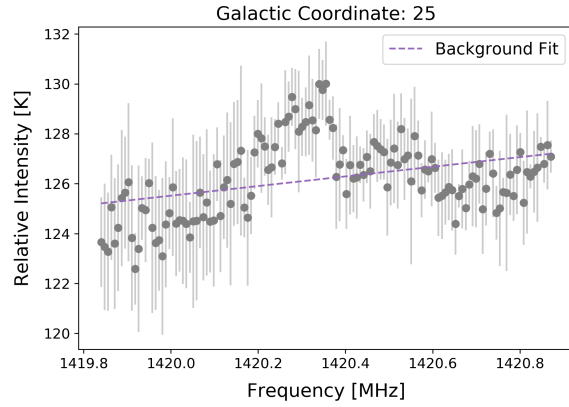
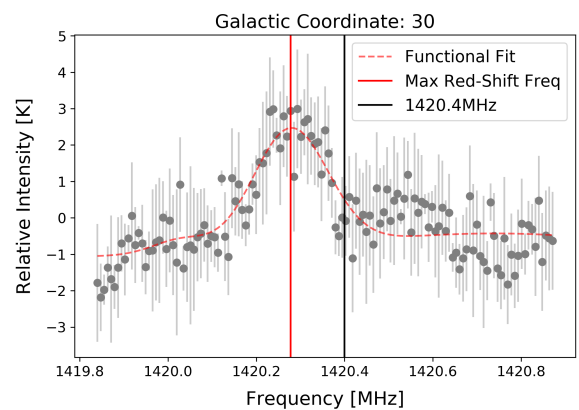
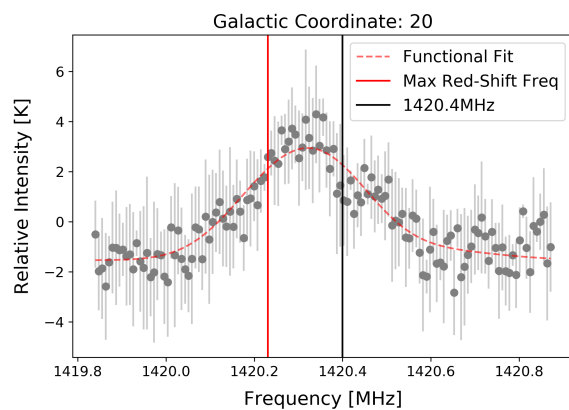
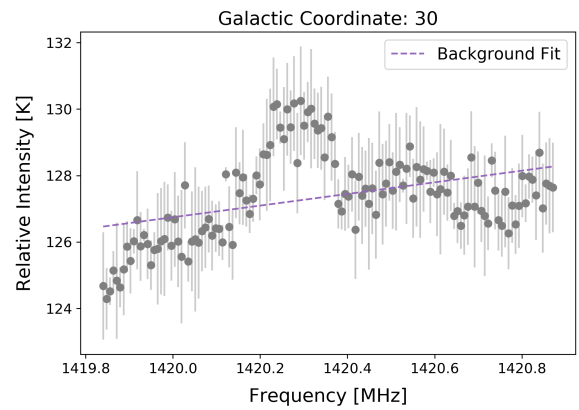
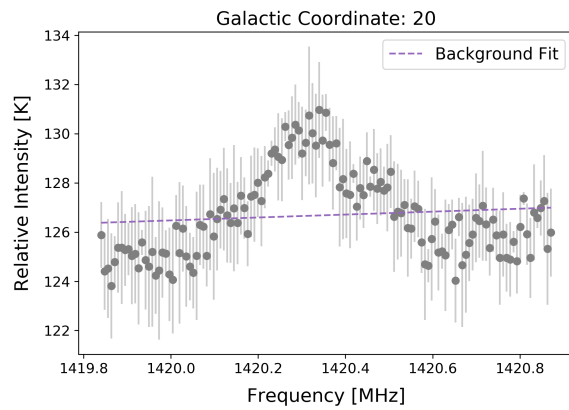
ACKNOWLEDGMENTS

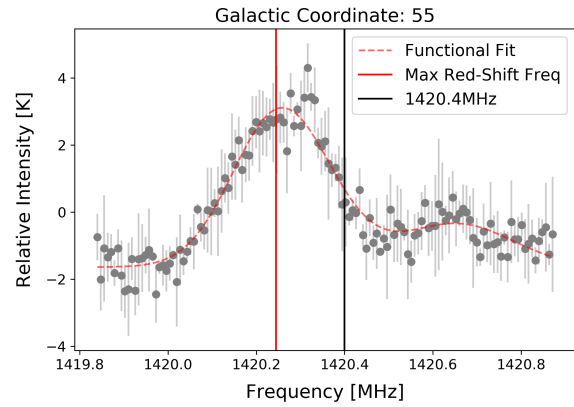
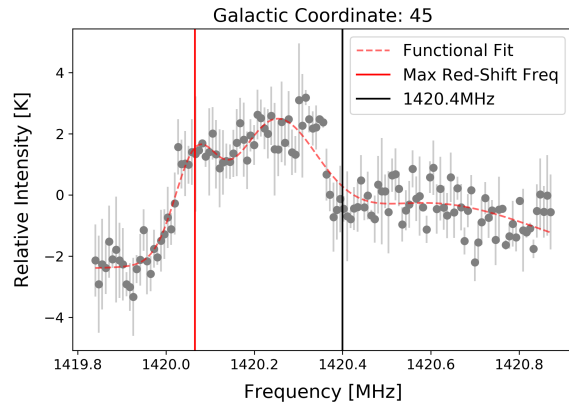
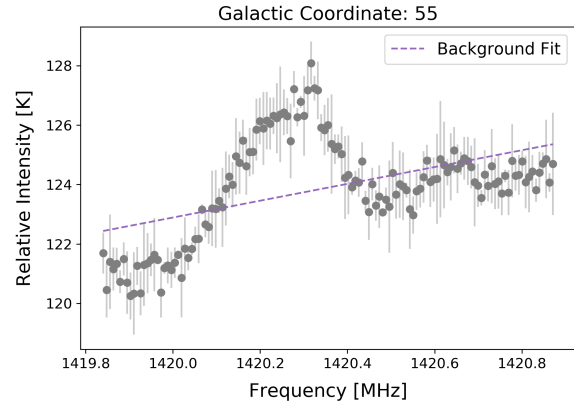
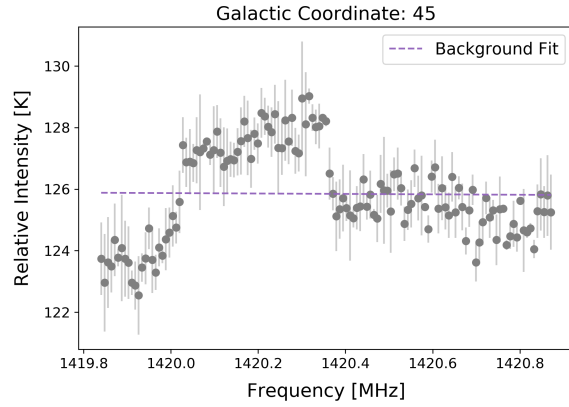
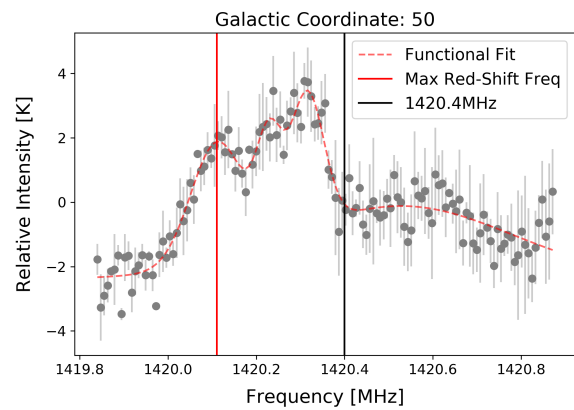
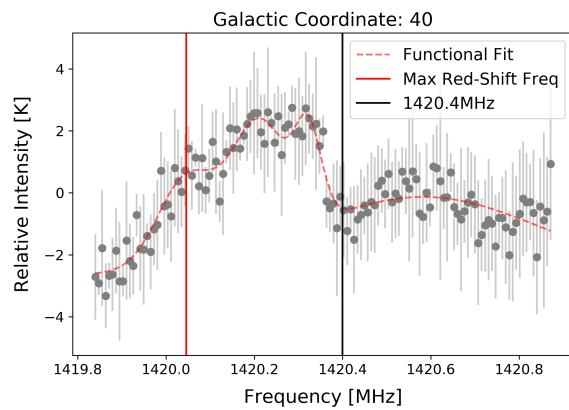
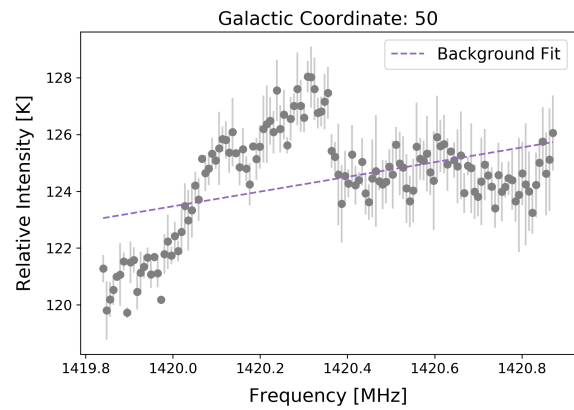
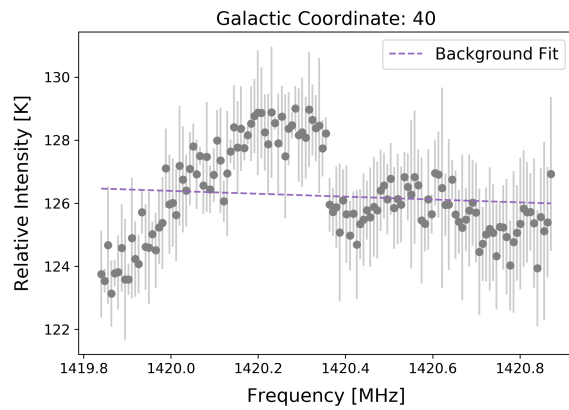
FV gratefully acknowledges Ghadah Alshalan's equal partnership, as well as the guidance and advice of the JLAB course staff and faculty.

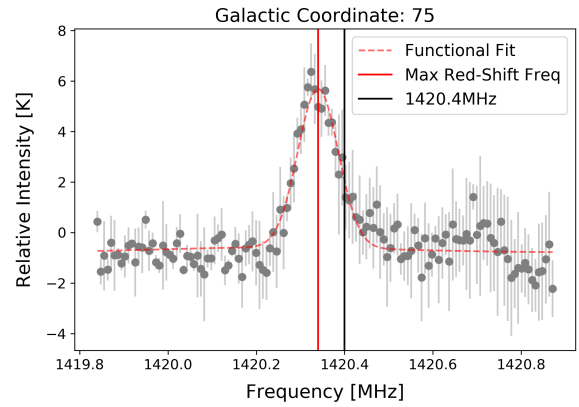
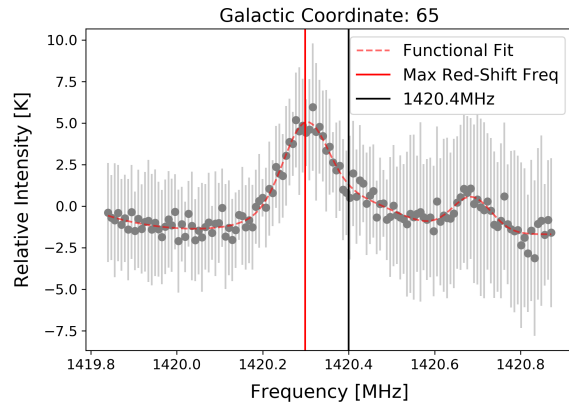
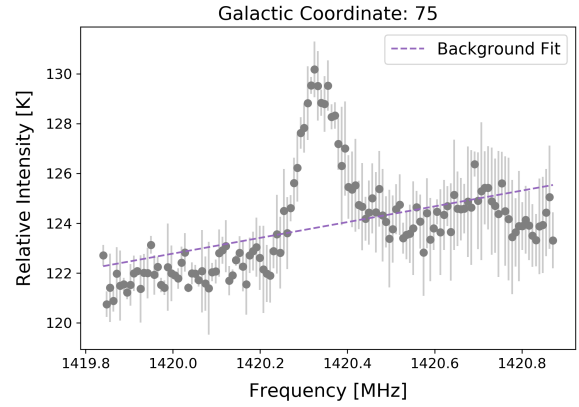
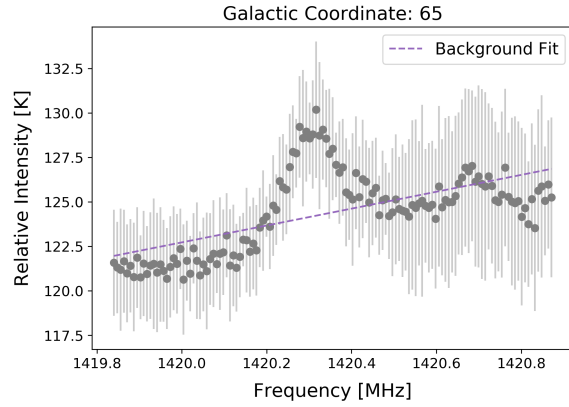
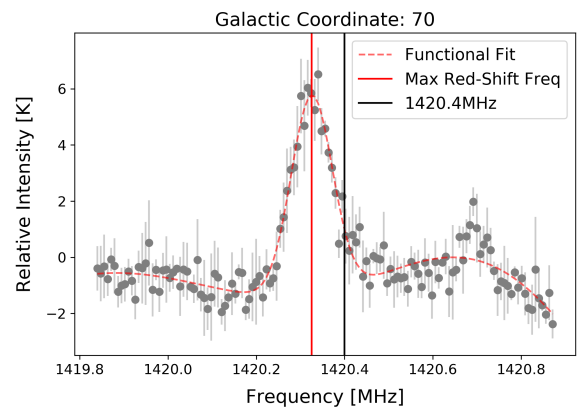
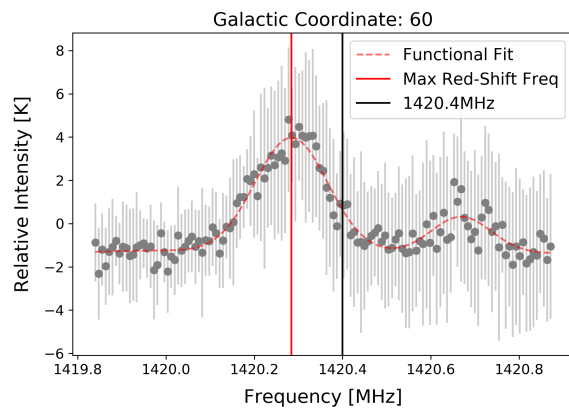
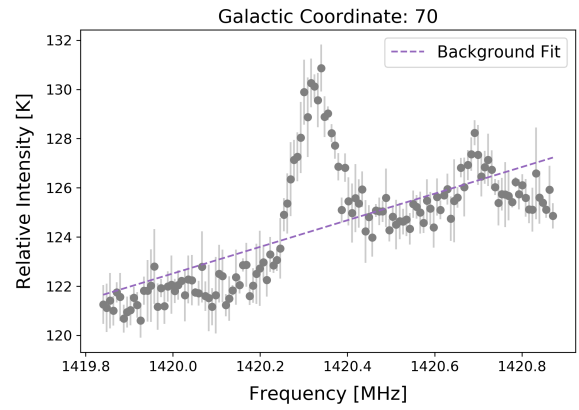
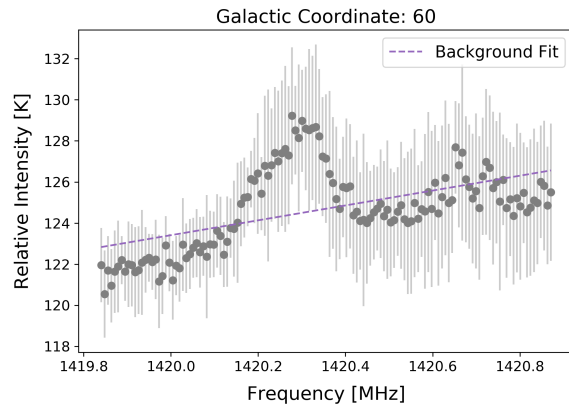
-
- [1] H. Poincare, Popular Astronomy **14**, 475 (1906).
 - [2] P. W. Hodge, “The structure and dynamics of the milky way galaxy,” (2019).
 - [3] Vanhollebeke, E., Groenewegen, M. A. T., and Girardi, L., *A&A* **498**, 95 (2009).
 - [4] G. Jungman, M. Kamionkowski, and K. Griest, Physics Reports **267**, 195 (1996).
 - [5] M. I. T. Physics, “Jlab 21cm radio-astrophysics manual,” .

Appendix A: Background & Frequency Fits









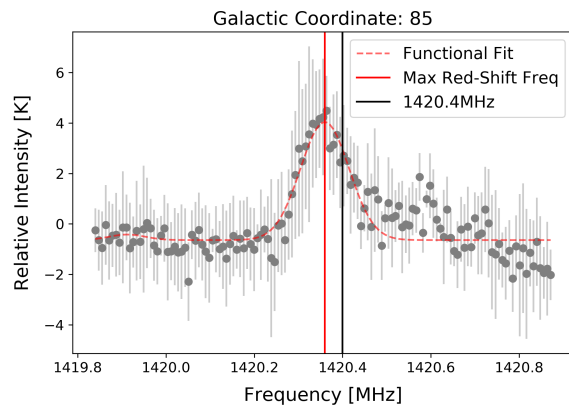
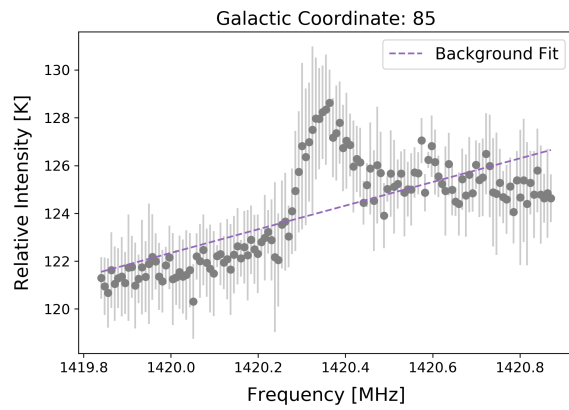
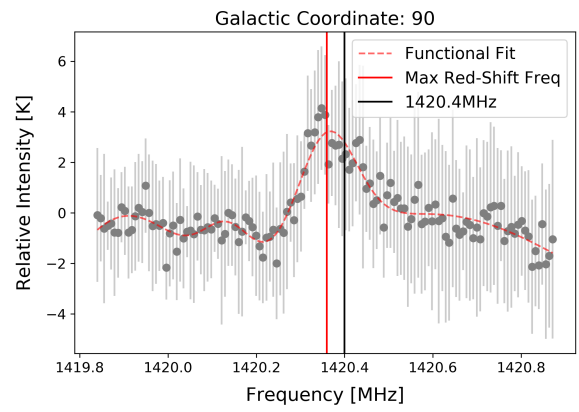
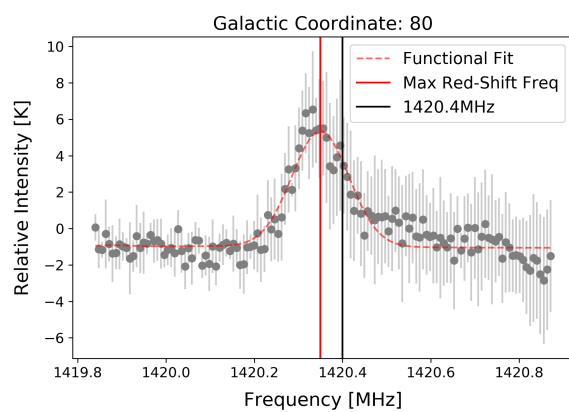
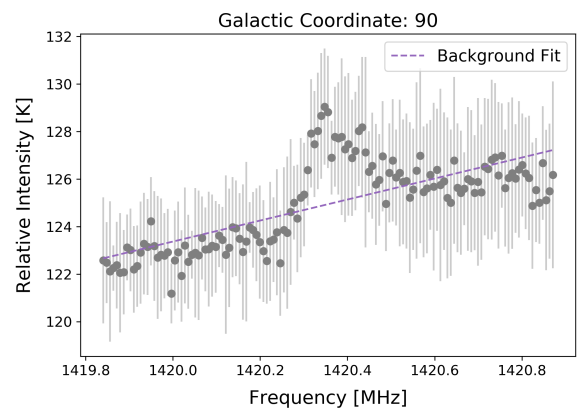
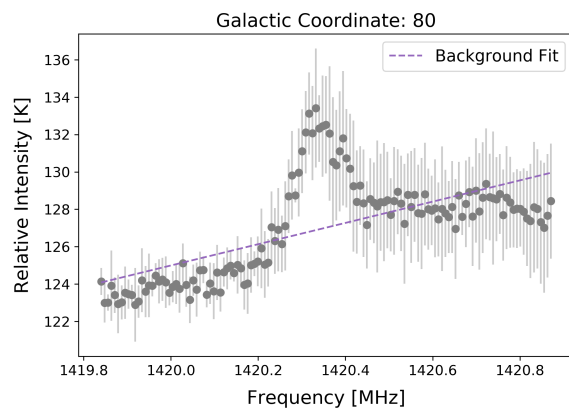


TABLE II. Linear fit results for background noise subtraction. Note that all fits have 132 degrees of freedom.

GC	Slope [$\frac{K}{MHz}$]	Offset [K]	χ^2	χ_r^2	$Pr(\chi^2)$
0°	4.04 ± 0.50	-5605.50 ± 708.35	3013.85	22.83	0
5°	2.44 ± 0.59	-3341.27 ± 832.41	92.43	0.70	1
10°	3.08 ± 0.70	-4246.38 ± 992.27	150.77	1.14	0.9964
15°	2.04 ± 0.61	-2775.57 ± 871.21	23009.14	174.31	0
20°	0.59 ± 0.50	-715.16 ± 710.40	297.91	2.27	0
25°	1.93 ± 0.41	-2617.53 ± 586.39	144.76	1.10	0.2112
30°	1.75 ± 0.35	-2359.97 ± 498.22	245.74	1.86	0
35°	1.75 ± 0.35	-2359.97 ± 498.22	245.74	1.86	0
40°	-0.45 ± 0.42	772.36 ± 593.11	538.35	4.08	0
45°	-0.07 ± 0.44	221.43 ± 624.08	1937.99	14.68	0
50°	2.59 ± 0.48	-3556.61 ± 679.29	3525.54	26.71	0
55°	2.83 ± 0.44	-3896.92 ± 627.39	1322.05	10.02	0
60°	3.62 ± 0.49	-5013.65 ± 692.11	54.97	0.42	0.9999
65°	4.75 ± 0.53	-6615.87 ± 756.86	53.94	0.41	0.9999
70°	5.41 ± 0.52	-7558.82 ± 737.00	1335.24	10.12	0
75°	3.16 ± 0.52	-4367.35 ± 742.32	38222.68	289.57	0
80°	5.70 ± 0.58	-7965.24 ± 829.00	185.03	1.40	0.0016
85°	4.94 ± 0.43	-6898.36 ± 609.33	115.42	0.87	0.8473
90°	4.42 ± 0.37	-6153.16 ± 527.79	41.60	0.32	0.9999

TABLE III. Four Gaussians and a linear offset fit results for determining max red shift. Note that all fits have 119 degrees of freedom. A , B , C , and D are Gaussian amplitudes [units=K]. σ and μ correspond to the Gaussian spread and mean, respectively [units=MHz]. Uncertainties for the fit parameters are left out because they are very small and do not contribute significantly to the final result (uncertainty dominated by other quantities described in the paper). The maximally red-shifted frequency is highlighted in pink for each galactic coordinate.

GC	A	σ_A	μ_A	B	σ_B	μ_B	C	σ_C	μ_C	D	σ_D	μ_D	offset	χ^2	χ_r^2	$Pr(\chi^2)$
0°	32.96	0.00	1419.82	0.82	0.07	1419.19	31.53	0.04	1419.62	0.70	0.05	1420.36	-0.68	458.40	3.85	0
5°	0.02	0.00	1419.86	0.12	0.03	1420.18	0.97	0.06	1420.33	0.17	0.04	1420.48	-1.23	17.15	0.14	1
10°	0.02	0.00	1419.89	0.02	0.00	1420.11	1.31	0.08	1420.30	0.33	0.05	1420.45	-1.6	14.30	0.12	1
15°	0.16	0.04	1419.86	1.88	0.17	1420.28	0.34	0.05	1420.29	2673.16	2.32	1428.24	-3.83	4939.22	41.51	0
20°	6.09	0.12	1419.99	0.61	0.11	1420.23	0.85	0.11	1420.37	0.13	0.14	1420.61	-1.54	93.80	0.79	0.9574
25°	0.00	0.12	1419.96	0.46	0.09	1420.26	0.56	0.13	20.37	0.06	0.17	1420.63	-1.03	61.65	0.52	0.9999
30°	0.00	0.07	1419.87	0.06	0.06	1420.03	0.70	0.09	1420.28	0.56	0.35	1420.74	-1.08	128.50	1.08	0.2600
35°	0.00	0.07	1419.87	0.06	0.06	1420.02	0.70	0.09	1420.28	0.57	0.35	1420.74	-1.08	128.50	1.08	0.2600
40°	0.45	0.06	1420.05	0.64	0.06	1420.21	0.20	0.03	1420.32	1.74	0.27	1420.58	-2.67	41.95	0.35	0.9999
45°	0.35	0.05	1420.07	0.97	0.10	1420.24	0.00	0.14	1420.37	1.39	0.26	1420.59	-2.42	428.77	3.60	0
50°	0.55	0.06	1420.11	0.22	0.03	1420.23	0.40	0.04	1420.31	1.44	0.25	1420.53	-2.39	331.64	2.79	0
55°	0.00	0.13	1419.98	1.11	0.10	1420.24	0.19	0.09	1420.35	0.42	0.13	1420.65	-1.63	161.20	1.35	0.0060
60°	0.04	0.13	1419.97	1.11	0.08	1420.28	0.00	0.10	1420.33	0.29	0.07	1420.67	-1.37	6.77	0.06	1
65°	3.40e8	0.82	1414.80	0.78	0.13	1420.37	0.59	0.05	1420.30	0.25	0.05	1420.69	-1.70	1.06	0.03	1
70°	2.19	1.27	1420.74	6.54	0.29	1420.75	15.05	0.53	1419.86	0.83	0.05	1420.33	-12.03	179.14	1.51	0.0003
75°	0.00	0.11	1420.04	0.12	0.26	1420.26	0.00	0.26	1420.05	0.72	0.05	1420.34	-0.79	2533.81	21.29	0
80°	0.01	0.06	1419.87	0.06	0.26	1420.18	0.00	0.21	1420.01	1.03	0.06	1420.35	-0.79	28.71	0.24	0.9999
85°	34.59	0.02	1419.69	5.68	0.06	1419.40	0.022	0.04	1419.91	0.64	0.06	1420.36	-0.64	67.84	0.57	0.9999
90°	1.72	0.14	1419.89	0.26	0.06	1420.13	0.73	0.06	1420.36	5.04	0.35	1420.59	-5.78	9.13	0.08	1